Non-Kitaev versus Kitaev honeycomb cobaltates

Xiaoyu Liu[1] and Hae-Young Kee[1,2,*]

[1]*Department of Physics, University of Toronto, Ontario, Canada M5S 1A7*

[2]*Program in Quantum Materials, Canadian Institute for Advanced Research, Toronto, Ontario, Canada M5G 1M1*

(Received 7 November 2022; accepted 31 January 2023; published 16 February 2023)

Recently, honeycomb cobaltates with $3d^7$ were proposed to display Kitaev physics despite weak spin-orbit coupling. However, other theoretical and experimental works found leading XXZ Heisenberg and negligible Kitaev interactions in $BaCo_2(AsO_4)_2$ (BCAO), which calls for further study to clarify the origin of the discrepancies. Here we derive the analytical expressions of the spin model using strong-coupling perturbation theory. With tight-binding parameters obtained with *ab initio* calculations for idealized honeycomb BCAO, we find that the largest intraorbital t_{2g}-t_{2g} exchange path, which was assumed to be small in the earlier theory proposal, leads to a ferromagnetic (FM) Heisenberg interaction. This becomes the dominant interaction, as other t_{2g}-e_g and e_g-e_g contributions almost cancel each other. Exactly the same assumed-to-be-small channel also generates an antiferromagnetic Kitaev interaction, which then cancels the FM Kitaev interaction from t_{2g}-e_g paths, resulting in a small Kitaev interaction. Under the trigonal distortion, the preeminent isotropic Heisenberg becomes an anisotropic XXZ model, as expected, which is the case in BCAO. However, when t_{2g}-e_g and intraorbital t_{2g}-t_{2g} hoppings are similar in size such as in $Na_3Co_2SbO_6$, the Kitaev interaction may become comparable to the Heisenberg interaction. A way to achieve the Kitaev cobaltates is also discussed.

DOI: 10.1103/PhysRevB.107.054420

I. INTRODUCTION

The Kitaev model, which consists of bond-dependent Ising interactions on the honeycomb lattice, is exactly solvable, and its ground state is the Kitaev spin liquid (KSL) with unusual excitations [1]. Due to the bond-dependent interaction character, its materialization requires angular momentum and spin degrees of freedom and their couplings, i.e., spin-orbit coupling (SOC) [2]. There has been a surge of studies on Kitaev candidate materials which may exhibit the KSL. The first proposed candidate was a group of $5d^5$ iridium oxides [2–4]. Later, α-$RuCl_3$ [5–8] with $4d^5$ was suggested to host the dominant Kitaev interaction despite the reduced SOC compared to iridates [7]. The single hole on t_{2g} orbitals has spin $S = 1/2$ and pseudoangular momentum $L_{\text{eff}} = 1$, giving rise to the $J_{\text{eff}} = 1/2$ doublet under strong SOC. The indirect exchange processes of $J_{\text{eff}} = 1/2$ via p orbitals lead to the Kitaev interaction [2].

However, these candidate materials are magnetically ordered at low temperatures [3,4,9–14]. This suggests that additional exchange interactions other than the Kitaev interaction are present. In particular, the Heisenberg interaction arising from direct hopping between d orbitals is non-negligible [15,16]. In addition, another bond-dependent interaction known as the Γ interaction [17] is significant in $4d$ and $5d$ materials. In real materials further interactions may appear, such as the Γ' interaction, which is generated by trigonal distortions [18].

Thus, a battle among the symmetry-allowed Kitaev (K), Heisenberg (J), Γ, and Γ' interactions determines the Kitaev materials in which the Kitaev interaction dominates. To build the Kitaev-dominant systems, Liu and Khaliullin [19] and Sano *et al.* [20] proposed to use materials with less extended $3d$ orbitals, as they may have a smaller d-d hopping integral. They suggested $3d^7$ cobaltates would be good candidates despite small SOC in $3d$ systems. The $3d^7$ systems have one hole in t_{2g} (t_{2g}^5) and two holes in e_g (e_g^2), leading to a total spin $S = 3/2$ and total angular momentum $L = 1$. With SOC, the lowest state is $J_{\text{eff}} = 1/2$. It was shown that the t_{2g}-e_g channels generate large antiferromagnetic (AFM) J and ferromagnetic (FM) K interactions. After taking the e_g-e_g exchange contribution, a cancellation of the Heisenberg interaction occurs, which makes the Kitaev interaction dominant. The t_{2g}-t_{2g} contributions to J and K were negligible; see Fig. 2 in Ref. [21].

Motivated by the proposal above, several theoretical and experimental works have been carried out on various rhombohedral cobaltates [22–32]. Theoretical studies found that $BaCo_2(AsO_4)_2$ (BCAO) is better described by the XXZ model with significant third nearest neighbor (NN) Heisenberg (J_3) interactions but negligible Kitaev interactions [33–36], similar to an earlier study on $BaCo_2(PO_4)_2$ (BCPO) [37]. More recently, a combined experimental and theoretical work [36] compared the two scenarios, XXZ-J-J_3 and $JK\Gamma\Gamma'$ models, in detail for BCAO. Using these models, the authors fit high-field magnon dispersion obtained by inelastic neutron scattering measurement and showed that the former model fits the experimental data well rather than the latter. These works together question whether cobaltates fall into the Kitaev candidates and call for a closer inspection of how the exchange processes add up or cancel out each other.

In this work we investigate the exchange processes for a $3d^7$ electron configuration using the strong-coupling perturbation theory and *ab initio* calculations to address the origin

*hykee@physics.utoronto.ca

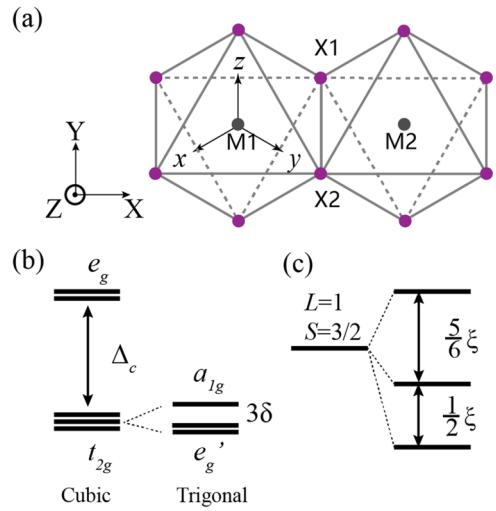

FIG. 1. (a) Crystal structure for an edge-sharing honeycomb octahedral lattice, where M and X represent the transition metal (Co) and ligand (such as AsO_4), respectively. The local octahedral coordinates (xyz) and the global basis (XYZ) are shown. (b) Splittings of $3d^7$ orbitals under cubic (Δ_c) and trigonal (δ) crystal fields. (c) Energy level splittings of $L=1$, $S=\frac{3}{2}$ states under SOC ξ.

of the discrepancies among the previous works on BCAO. Starting from the ideal honeycomb lattice, we find that an *intraorbital* hopping channel (denoted by t_3) among the t_{2g}-t_{2g} exchange paths, assumed to be negligible in Refs. [19,20], is significant. Taking into account this exchange path together with Hund's coupling, the FM Heisenberg interaction is greatly boosted. This becomes the major Heisenberg interaction because other contributions from the t_{2g}-e_g and e_g-e_g paths almost cancel each other. Exactly the same assumed-to-be-small channel also generates the AFM Kitaev interaction, which then cancels the proposed FM Kitaev interaction from the t_{2g}-e_g path, resulting in a small Kitaev interaction. We confirm a dominant FM Heisenberg interaction in BCAO. Under the trigonal distortion, the isotropic Heisenberg interaction becomes an anisotropic XXZ interaction which dominates over other interactions. On the other hand, in $Na_3Co_2SbO_6$ (NCSO), the t_{2g}-e_g hopping becomes comparable to t_3 [31], which makes the FM Kitaev interaction approximately as large as the Heisenberg interaction.

The rest of this paper is organized as follows. In Sec. II we review the on-site Hamiltonian of the Co honeycomb. In Sec. III we introduce the various direct and indirect hoppings considered in our model. Section IV introduces the derivation of the spin Hamiltonian and gives analytical expressions for various exchange interactions. We present *ab initio* parameters and results for BCAO as an example in Sec. V. The effect of the trigonal distortions is discussed in Sec. VI, and finally, the discussion and conclusion are given in Sec. VII.

II. ON-SITE HAMILTONIAN

The structure of honeycomb cobaltates is similar to other edge-sharing octahedral honeycomb materials [see Fig. 1(a)]. For these materials, the on-site Hamiltonian for multiorbital d^7 is expressed by

$$H_{\text{onsite}} = H_{\text{Coulomb}} + H_{\text{CFS}} + H_{\text{SOC}}, \tag{1}$$

where H_{Coulomb}, H_{CFS}, and H_{SOC} represent the electron-electron interactions, the crystal field splitting (CFS), and the SOC, respectively. The total Hamiltonian of the system includes both H_{onsite} and the tight-binding Hamiltonians discussed in Sec. III. For simplicity, the isotropic Kanamori interaction [38] is used and is a good approximation of the full Coulomb interaction with three- and four-orbital effects [39–42]. Within this approximation, the H_{Coulomb} is written as

$$\begin{aligned} H_{\text{Coulomb}} = {} & U\sum_a n_{a\uparrow}n_{a\downarrow} + \frac{U'}{2}\sum_{a\neq b,\sigma,\sigma'} n_{a\sigma}n_{b\sigma'} \\ & - \frac{J_H}{2}\sum_{a\neq b,\sigma\sigma'} c^\dagger_{a\sigma}c^\dagger_{b\sigma'}c_{b\sigma}c_{a\sigma'} \\ & + J_H\sum_{a\neq b} c^\dagger_{a\uparrow}c^\dagger_{a\downarrow}c_{b\downarrow}c_{b\uparrow}, \end{aligned} \tag{2}$$

where a and b represent the orbitals and σ and σ' are the spin $\uparrow$ and $\downarrow$. U and U' are intra- and interorbital Coulomb interactions, respectively, and J_H is the Hund's coupling.

There are two kinds of CFSs in edge-sharing octahedral honeycomb lattices. One is the cubic CFS due to the octahedral cage formed by oxygen atoms [see Fig. 1(b)]. It is usually around 1 eV and is comparable to the Hund's coupling J_H for $3d$ orbitals. The other is the trigonal CFS induced by the trigonal distortion of the two-dimensional (2D) honeycomb lattice [compression or elongation of the octahedral cages along Z direction shown in Fig. 1(a)]. This is usually small (from several meV to several tens of meV). Combining the two crystal field effects, H_{CFS} is given by

$$\begin{aligned} H_{\text{CFS}} &= H_{\text{cubic}} + H_{\text{trig}} \\ &= \begin{pmatrix} \Delta_c & 0 & 0 & 0 & 0 \\ 0 & \Delta_c & 0 & 0 & 0 \\ 0 & 0 & 0 & \delta & \delta \\ 0 & 0 & \delta & 0 & \delta \\ 0 & 0 & \delta & \delta & 0 \end{pmatrix} \end{aligned} \tag{3}$$

in the basis of $(d_{x^2-y^2}, d_{3z^2-r^2}, d_{yz}, d_{xz}, d_{xy})$. Δ_c is the splitting between t_{2g} and e_g orbitals by the cubic CFS, and δ is the trigonal distortion.

Due to a large Hund's coupling, $3d^7$ forms a high spin state with total angular momentum $L=1$ and total spin $S=3/2$. Under $H_{\text{SOC}} = \lambda\mathbf{L}\cdot\mathbf{S}$, the lowest states form a $\tilde{J}=\frac{1}{2}$ doublet [see Fig. 1(b)]. Using the basis of $|S_z, L_z\rangle$, $|\tilde{J}_z\rangle = \pm|\frac{1}{2}\rangle$ are given by [19–21,35,43]

$$\begin{aligned} \left|+\frac{\tilde{1}}{2}\right\rangle &= \frac{1}{\sqrt{2}}\left|\frac{3}{2},-1\right\rangle - \frac{1}{\sqrt{3}}\left|\frac{1}{2},0\right\rangle + \frac{1}{\sqrt{6}}\left|-\frac{1}{2},1\right\rangle, \\ \left|-\frac{\tilde{1}}{2}\right\rangle &= \frac{1}{\sqrt{2}}\left|-\frac{3}{2},1\right\rangle - \frac{1}{\sqrt{3}}\left|-\frac{1}{2},0\right\rangle + \frac{1}{\sqrt{6}}\left|\frac{1}{2},-1\right\rangle. \end{aligned} \tag{4}$$

In this work, we use $H_{\text{SOC}} = \xi\sum_{i=1}^3 \mathbf{l}_i\cdot\mathbf{s}_i$, where ξ is the atomic SOC strength and $i=1$–3 counts the number of holes. The relation to $\lambda\mathbf{L}\cdot\mathbf{S}$, where $\mathbf{L}=\sum_i \mathbf{l}_i$ and $\mathbf{S}=\sum_i \mathbf{s}_i$, is

$\lambda = \xi/3$ because there are three holes [44]. The SOC-induced energy splittings are shown in Fig. 1(c).

III. EXCHANGE PATHS

Having set the on-site Hamiltonian, we now consider the hopping paths to determine exchange processes. As shown in Fig. 1(a), bond M_1-M_2 has C_{2v} local symmetry, and the symmetry-allowed hopping integrals for the ideal honeycomb lattice are given by

$$T_{ij}^{dd} = \begin{pmatrix} t_5 & 0 & 0 & 0 & 0 \\ 0 & t_4 & 0 & 0 & t_6 \\ 0 & 0 & t_1 & t_2 & 0 \\ 0 & 0 & t_2 & t_1 & 0 \\ 0 & t_6 & 0 & 0 & t_3 \end{pmatrix} \tag{5}$$

in the basis of $(d_{x^2-y^2}, d_{3z^2-r^2}, d_{yz}, d_{xz}, d_{xy})$. Here dd refers to the hopping integral between d and d orbitals, and i and j are nearest neighbor Co sites. t_1, t_3, t_4, and t_5 are intraorbital direct hoppings between $d_{yz/xz}$, d_{xy}, $d_{3z^2-r^2}$, and $d_{x^2-y^2}$, respectively. t_2 is the hopping between d_{yz} and d_{xz}, which includes both direct and indirect hoppings. t_6 is the hopping between t_{2g} and e_g manifolds and also includes both direct and indirect hoppings. Hoppings of other bonds are related to the z bond by C_3 symmetry.

The symmetry- allowed p-d hopping integrals between d orbitals at site i and p orbitals in anions at site j are parameterized as [take bond M_1-X_1 as an example; see Fig. 1(a)]

$$T_{ij}^{dp} = \begin{pmatrix} \frac{\sqrt{3}}{2}t_{pd\sigma} & 0 & 0 \\ -\frac{1}{2}t_{pd\sigma} & 0 & 0 \\ 0 & 0 & 0 \\ 0 & 0 & t_{pd\pi} \\ 0 & t_{pd\pi} & 0 \end{pmatrix} \tag{6}$$

in the basis of (p_x, p_y, p_z) and $(d_{x^2-y^2}, d_{3z^2-r^2}, d_{yz}, d_{xz}, d_{xy})^\dagger$. The other bond, M_1-X_2, is related by C_2 symmetry about the X axis. These hopping parameters can be obtained from density functional theory (DFT) calculations once a target system is chosen, as we will discuss in Sec. V.

IV. SPIN MODEL

With both the on-site and intersite Hamiltonians, we derive the spin model using the strong-coupling perturbation theory. For the edge-sharing ideal honeycomb octahedral lattice, the generic NN spin model is given by [17]

$$H_{\text{spin}} = \sum_{\langle ij\rangle \in \alpha\beta(\gamma)} J\mathbf{S}_i \cdot \mathbf{S}_j + KS_i^\gamma S_j^\gamma + \Gamma\left(S_i^\alpha S_j^\beta + S_i^\beta S_j^\alpha\right). \tag{7}$$

For a bond connecting the nearest neighbor sites i and j, we distinguish one spin direction γ, labeling the bond $\alpha\beta(\gamma)$, where α and β are the two remaining directions. For example, for the z bond, $\gamma = z$, while α and β take x and y. J, K, and Γ are the isotropic Heisenberg, bond-dependent Kitaev, and bond-dependent off-diagonal terms, respectively. Other bond-dependent off-diagonal terms such as Γ' are forbidden in ideal circumstances. To determine the relative strength among them, we present three different types of exchange processes and show which combinations determine the major interaction.

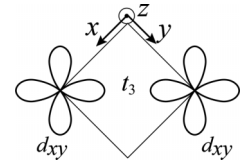

FIG. 2. The dominant second-order intersite U process is the direct hopping between neighboring d_{xy} orbitals.

A. Intersite U process

A virtual hopping of one d electron between neighboring Co atoms through a second-order process (d^7d^7-d^6d^8-d^7d^7 or d^7d^7-d^8d^6-d^7d^7) can lower the total energy and thus contributes to the spin Hamiltonian. The analytical expressions of spin interactions from all second-order processes are listed in Table IV in Appendix B.

The major difference between our finding and the conclusion from Refs. [19,21] is the strength of the t_3 hopping integral. In Refs. [19,21], it was assumed that t_3 (t' in their notation) is negligible based on less extended $3d$ orbitals. However, since $3d$ systems have a smaller lattice constant, we expect a large t_3 compared to other hopping integrals. Indeed, the large t_3 hopping integral was also reported in a previous work [35] on BCAO. In the same study, the dependence of the large t_3 hopping integral on the Co-Co bond length in various other cobaltates was also examined [35].

The t_3 associated exchange process shown in Fig. 2 can be summarized by the following Heisenberg and Kitaev interactions:

$$J = \frac{2}{243}\left(-\frac{27}{U-3J_H} + \frac{43}{U+J_H} + \frac{8}{U+4J_H}\right)t_3^2,$$
$$K = \frac{2}{81}\left(\frac{3}{U-3J_H} - \frac{7}{U+J_H} - \frac{2}{U+4J_H}\right)t_3^2. \tag{8}$$

Hund's coupling enters into these expressions explicitly due to the energy differences between intermediate state d^6d^8 (or d^8d^6) and the initial state (d^7d^7). When J_H approaches zero, the above equations reduce to $J = \frac{16t_3^2}{81U}$ and $K = -\frac{3}{4}J$, respectively, consistent with Eq. (7) in Ref. [19]. When $J_H/U > 0.15$, the sign of J changes, and it grows quickly due to the large t_3^2, implying a dominant FM Heisenberg interaction. This precise path leads to the AFM Kitaev interaction. However, as we will show below, this weakens the FM Kitaev interaction from the t_{2g}-e_g paths. The combination of these two results, i.e., incomplete cancellation of J and almost complete cancellation of K, is a key reason why some cobaltates do not fall into the Kitaev materials.

As we will show later, the Heisenberg terms from other exchange paths together further enhance the FM character. Our work implies that a realization of Kitaev materials in $3d$ transition metals is unlikely, as it requires fine tuning to reduce the intraorbital hopping integral t_3.

Our spin interactions from the t_2 and t_6 processes are consistent with the results reported in Ref. [20]. These channels play a minor role in the second-order processes. The Kitaev interaction has both FM and AFM contributions from different second-order processes. The Γ interaction involves two cross terms inside t_{2g} manifolds. The expression for Γ and the full

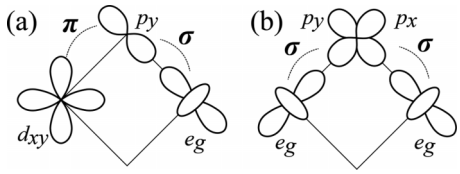

FIG. 3. The dominant two-hole processes with two holes in (a) the same orbital and (b) different orbital.

expressions for J and K from other hopping paths are listed in Table IV in Appendix B.

B. Two-hole process

Due to the strong p-d hybridization, contributions from p orbitals are also important. The processes involving p orbitals start at fourth order to introduce coupling between neighboring Co atoms. The single-hole p orbital mediated hopping processes are already included in the effective d-d hopping integral, i.e., the intersite U process. The leftover fourth-order processes are the two-hole and cyclic exchange processes, which require 34 orbitals, as discussed below.

The two-hole processes include intermediate states when the two holes are located at one ligand atom simultaneously. The two holes can be in either the same orbital or different orbitals. The former leads to AFM Heisenberg contributions, and the latter prefers FM contributions due to Hund's coupling of the p orbitals J_{Hp}. The analytical expressions for two-hole processes are listed in Appendix B. When expanded to the linear order of J_{Hp}, our results are consistent with Ref. [19]. The contributions from the t_{2g}-t_{2g}, t_{2g}-e_g, and e_g-e_g groups are indicated by their hopping integrals $t^4_{pd\pi}$, $t^2_{pd\pi}t^2_{pd\sigma}$, and $t^4_{pd\sigma}$, respectively. The two dominant two-hole processes are illustrated in Fig. 3. Figure 3(a) shows an intermediate state configuration that is capable of accommodating two holes in the same orbital. It requires one of the holes to come from the t_{2g} orbitals and the other to come from the e_g orbitals, and the two holes have opposite spins, leading to an AFM Heisenberg term. The resulting form of the exchange interaction captures this process. For example, the Heisenberg and Kitaev interactions from the two-hole contribution denoted by J^{2h} and K^{2h} contain $t^2_{pd\pi}t^2_{pd\sigma}(\frac{1}{\Delta_{pd}}+\frac{1}{\Delta_{pd}+\Delta_c})^2$. Here the numerator $t^2_{pd\pi}t^2_{pd\sigma}$ indicates the hoppings between $t_{2g}(e_g)$ and p orbitals, while the denominator shows the energy costs of such intermediate states, Δ_{pd} for an electron hopping from t_{2g} to p orbitals and $\Delta_{pd}+\Delta_c$ for hopping from e_g to p orbitals. Figure 3(b) shows a configuration with two holes in different orbitals. A FM contribution is expected as the two holes prefer to align the spins parallel due to Hund's coupling. Notice that the e_g-e_g processes do not have Kitaev contributions. This is due to the cubic CFS that quenches the orbital angular momentum of the e_g orbitals. As analyzed above, the two processes shown in Fig. 3 have opposite signs and partially cancel each other.

C. Cyclic exchange process

Another fourth-order perturbation process is the cyclic exchange process, as shown in Fig 4(a). It has an intermediate state when each of the two ligand atoms have one hole. Due to the property of identical particles, we cannot distinguish

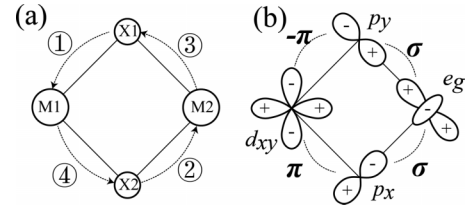

FIG. 4. (a) The paths for cyclic exchange processes. The related paths are obtained by interchanging 12 and/or 3↔4, as well as reversing the cycle direction. (b) The dominant cyclic exchange process.

the two holes, and thus, this is a purely quantum mechanical process. The dominant process is illustrated in Fig 4(b) and involves both t_{2g} and e_g orbitals. As seen in Fig. 4(b), the geometric effects lead to opposite signs for the hopping integrals involved in the π process between the p_x/p_y and $t_{2g}d_{xy}$ orbitals. As a result, the Heisenberg interaction in cyclic exchange processes always has a negative sign, indicating ferromagnetic behavior.

Combining all the significant processes up to fourth order, only one process [Fig. 3(a)] can give rise to the AFM Heisenberg interaction. Usually, this process has a magnitude comparable to that of other paths shown in Fig. 3(b) and/or Fig. 4(b). Thus, the perfect cancellation of the Heisenberg interaction cannot be expected generally.

V. APPLICATION TO BCAO

To apply the above theory, we obtain tight-binding parameters for BCAO using DFT calculations. The calculation is performed with the Vienna Ab initio Simulation Package (VASP) [45] with the projector augmented wave [46] potential and Perdew-Burke-Ernzerhof [47] exchange-correlation functional. The cutoff energy of the plane wave basis is set to 400 eV. The k-point mesh is $5\times5\times5$. The hopping parameters are obtained with spin-unpolarized calculations without SOC. The WANNIER90 code [48] is used to build tight-binding models out of the DFT calculation. To discuss both second- and fourth-order perturbation processes, we build two Wannier models from purely d orbitals and from both p and d orbitals. The tight-binding parameters are provided in Appendix A, where hoppings in T_{dd} and T_{dp} are read out.

We confirm that t_3 is the largest hopping integral. We also note that the indirect hopping between d_{xz} and d_{yz} orbitals through p orbitals, i.e., some part of t_2 channels (t in Ref. [19]), cancels the direct hopping channel and is thus much smaller than t_3.

Using the tight-binding parameters and the exchange interactions obtained above, a set of exchange parameters for an idealized honeycomb BCAO is listed in Table I. Here we classify the various second- and fourth-order processes into three groups, depending on whether hoppings are between t_{2g}-t_{2g} orbitals, t_{2g}-e_g orbitals, or e_g-e_g orbitals. They are denoted by A, B, and C, respectively; 1, 2, and 3 represent second-order, two-hole, and cyclic exchange processes, respectively, following the same notation used in Ref. [19]. Note the dominant Heisenberg interaction but the almost cancellation of the Kitaev interaction from A1, B2, and B3.

TABLE I. Exchange interactions for the idealized honeycomb BCAO. We set $U = 6\,\text{eV}$, $J = 0.2\,U$, $U_p = 4\,\text{eV}$ $J_{Hp} = 1\,\text{eV}$, $\Delta_c = 0.9\,\text{eV}$, and $\Delta_{pd} = 3.5\,\text{eV}$. The SOC for Co atoms is 60 meV. Here 1, 2, and 3 are intersite, two-hole, and cyclic exchange processes, respectively. A, B, and C denote contributions from t_{2g}-t_{2g}, t_{2g}-e_g, and e_g-e_g processes, respectively.

	A1	B1	C1	A2	B2	C2	A3	B3	C3	Total
J	−5.79	0.04	0.45	0.17	14.37	−6.3	0.1	−11.75	0	−8.7
K	2.47	−0.2	0	0.71	−8.38	0	−1.03	5.87	0	−0.55
Γ	−0.56	0	0	0	0	0	0	0	0	−0.56

As expected from our analysis, the second-order intersite U process gives rise to a FM Heisenberg interaction. The only significant AFM Heisenberg interaction comes from the two-hole processes (B2) with two holes in the same orbital. The cancellation of Heisenberg interactions is incomplete. Tuning the local interaction parameters such as U and J_H can alter the numbers but does not affect the qualitative result that the Heisenberg interaction is dominant.

VI. TRIGONAL DISTORTION

The above results are limited to the ideal system where the $J_{\text{eff}} = \frac{1}{2}$ picture is intact. In materials like BCAO, the trigonal distortion is present, which modifies the ideal $J_{\text{eff}} = \frac{1}{2}$ picture. In this section, we present how the trigonal distortion alters the spin Hamiltonian and the relative strength of exchange interactions.

The trigonal distortion $H_{\text{trig}} = \delta(3L_Z^2 - 2)$ [21] breaks the $J_{\text{eff}} = \frac{1}{2}$ picture, but the lowest states are still doubly degenerate and isolated from other energy states for some ranges of the trigonal-distortion strength δ [35,43]. Since H_{trig} commutes with the Z component of the total angular momentum J_Z, where $Z = [111]$ in xyz coordinates [see Fig. 1 (a)], J_Z is preserved for a finite δ. It is useful to write the spin model in the XYZ coordinates.

The spin Hamiltonian in the global XYZ coordinates is written as (for the z bond)

$$H^z_{\text{spin}} = \begin{pmatrix} J_{XY} + D & E & F \\ E & J_{XY} - D & G \\ F & G & J_Z \end{pmatrix}. \tag{9}$$

Here we use the notation introduced in Ref. [33] where D and F correspond to A and $-\sqrt{2}B$ in Ref. [49], respectively, which are equivalent to J_{ab} and $-\sqrt{2}J_{ac}$ in Ref. [50]. When the C_{2v} symmetry along the Y axis is intact, $E = G = 0$.

Rotating the above Hamiltonian to the xyz coordinates, the model is given by the familiar $JK\Gamma\Gamma'$ with a small deviation if the C_{2v} symmetry is broken:

$$H^z_{\text{spin}} = \begin{pmatrix} J + \eta & \Gamma & \Gamma'_1 \\ \Gamma & J - \eta & \Gamma'_2 \\ \Gamma'_1 & \Gamma'_2 & J + K \end{pmatrix}. \tag{10}$$

Since the analytical expressions of the exchange interactions including the trigonal distortion are hard to derive, we present the numerical results in Tables II and III. From Table II we find the dominant FM XXZ Heisenberg terms (J_{XY} and J_Z) as expected. D, E, and F serve as additional anisotropic terms and are negligible. We also find that the contributions from fourth-order processes (process 2 and 3) are non-negligible compared with the intersite U second-order contribution (process 1). Converting to xyz coordinates, we find the FM Kitaev interactions are overall negligible, as shown in Table III. Here we ignore the distortion-induced hopping for simplicity [42,51], which we do not expect to change the main finding. The result is consistent with the analysis from the ideal case. Apart from the cancellation of the Kitaev term between different processes, the inclusion of the trigonal distortion further weakens the Kitaev term in each process. Since C_{2v} symmetry is intact, $\eta = 0$ and $\Gamma'_1 = \Gamma'_2$. Depending on how the layers are stacked, C_{2v} can be broken, leading to finite η and different Γ' (and a finite E and G), which are ignored in this study. Other bonds are related to the z bond by C_3 rotation.

VII. SUMMARY AND DISCUSSION

Kitaev materials refer to materials in which the Kitaev interaction dominates over other symmetry-allowed interactions. Recently, it was suggested that $3d^7$ honeycomb cobaltates are Kitaev candidates [19–21], which has extended our search for the KSL. However, the application of the proposal was questioned by other theoretical and experimental works on BCAO and BCPO [33–36]. We investigated a possible origin of the two different proposals, non-Kitaev vs Kitaev cobaltates.

The original proposal made by Liu and Khaliullin and Sano *et al.* [19,20] is based on the idea that the AFM Heisenberg interaction from the t_{2g}-e_g path and the FM Heisenberg interaction from the e_g-e_g path almost cancel out each other, while the t_{2g}-e_g channel generates a FM Kitaev interaction, resulting in the dominant Kitaev interaction. These theories assumed a negligible intraorbital t_3 hopping integral. Within our DFT calculations we found that t_3 is the largest hopping

TABLE II. Exchange interactions (in meV) under the trigonal distortion. Here 1, 2, and 3 are intersite, two-hole, and cyclic exchange processes, respectively. We use the same parameters as in the caption of Table I with the SOC of the Co atom equal to 60 meV and the trigonal field $\delta = 40$ meV.

	1	2	3	Total
J_{XY}	−6.91	7.66	−11.88	−11.13
J_Z	−1.59	2	−3.06	−2.65
D	−0.17	0.81	−0.28	0.35
E	0	0	0	0
F	0.01	−0.55	0.55	0.02
G	0	0	0	0

TABLE III. Exchange interactions (in meV) under the trigonal distortion in the xyz basis, converted from Table II.

	1	2	3	Total
J	−5.2	6.3	−9.24	−8.14
K	0.19	−1.58	0.91	−0.47
η	0	0	0	0
Γ	1.88	−2.17	2.92	2.63
Γ_1'	1.72	−1.75	2.88	2.85
Γ_2'	1.72	−1.75	2.88	2.85

integral in BCAO and BCPO, consistent with Ref. [35]. We also showed that the exchange path associated with t_3 turns the story around. The t_3 exchange channel generates FM Heisenberg and AFM Kitaev interactions. Combined with other contributions, the FM Heisenberg interaction from the t_3 path becomes the dominant interaction, while the Kitaev interactions from the t_3 and the t_{2g}-e_g paths almost cancel out each other. Applying our theory to BCAO, we found that t_3 is, indeed, the largest, consistent with [34], which seems to be the case for other cobaltates [35]. However, despite the largest t_3 hopping, the t_{2g}-e_g (denoted by t_6) hopping grows while t_3 decreases in NCSO [31]. In this case, the Kitaev interaction from the t_3 channel becomes weaker and cannot compensate the one from t_6, making the Kitaev interaction comparable to the Heisenberg interaction.

Under the trigonal distortion, the doublet is modified from $J_{\text{eff}} = \frac{1}{2}$. This leads to additional anisotropic spin interactions. Experimentally, BCAO exhibits strong anisotropic g factors [33], implying that the trigonal distortion is relatively strong compared with SOC for a Co atom. We find that the Heisenberg interaction becomes the XXZ type when the trigonal distortion is introduced, which is rather expected since the ideal limit has a dominant isotropic Heisenberg interaction. We did not consider the third NN Heisenberg interaction J_3, as our motivation was to find the origin of the debate over the dominant NN Kitaev vs Heisenberg interactions. The importance of J_3 can be found in Refs. [34–37].

While a material-dependent analysis is required to take into account the local environment such as bond lengths and bond angles, we expect that the significant NN FM Heisenberg interaction is common across the $3d^7$ cobaltates such as BCAO, BCPO, NCSO, and $Na_2Co_2TeO_6$ due to the large intraorbital hopping integral t_3 and Hund's coupling. However, a target Kitaev cobaltate can be engineered with effectively reduced intraorbital t_3 and enhanced p orbital mediated hoppings, which will move the system towards the dominant Kitaev regime, as proposed in Refs. [19,20]. Future theoretical and experimental works are needed to discover Kitaev honeycomb cobaltates.

ACKNOWLEDGMENTS

We thank D. Churchill, Y. B. Kim, and H. Liu for useful discussions. We also thank K. Ross for bringing BCAO and BCPO to our attention. We acknowledge support from the Natural Sciences and Engineering Research Council of Canada Discovery Grant No. 2022-04601. H.-Y.K. also acknowledges support from the Canadian Institute for Advanced Research and the Canada Research Chairs Program. Computations were performed on the Niagara supercomputer at the SciNet HPC Consortium. SciNet is funded by the Canada Foundation for Innovation under the auspices of Compute Canada, the Government of Ontario, Ontario Research FundResearch Excellence, and the University of Toronto.

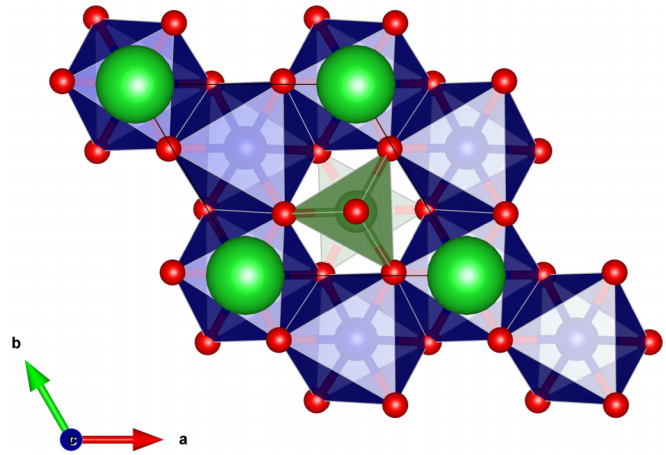

FIG. 5. The c-axis view of the Co-O honeycomb lattice of $BaCo_2(AsO_4)_2$. Blue, red, light green, and dark green balls correspond to Co, O, As, and Ba atoms.

APPENDIX A: CRYSTAL STRUCTURE FOR $BaCo_2(AsO_4)_2$

Honeycomb cobaltates are composed of stacking 2D honeycomb lattices formed by edge-sharing octahedrons. We show in Fig. 5 the structure of an example material, $BaCo_2(AsO_4)_2$. The most basic feature is the edge-sharing twin octahedrons, which we emphasized in Fig. 1(a). It is convenient that we choose d and p orbitals sitting at atom sites and pointing towards the local basis (xyz) as the starting point of our analysis.

APPENDIX B: TIGHT-BINDING PARAMETERS

We construct two tight-binding models for BCAO. One includes only d orbitals of the Co atom. There are in total 10 d orbitals in one unit cell. The on-site Hamiltonian as well as the hoppings between d-d orbitals obtained from DFT and Wannier calculations are (in meV)

$$H_d^{10} = \begin{pmatrix} 4850.77 & 0 & 7.75 & 8.45 & -16.2 \\ 0 & 4850.77 & 14.24 & -13.83 & -0.4 \\ 7.75 & 14.24 & 3952.74 & 38.87 & 38.87 \\ 8.45 & -13.83 & 38.87 & 3952.74 & 38.87 \\ -16.2 & -0.4 & 38.87 & 38.87 & 3952.74 \end{pmatrix},$$

$$T_{dd}^{10} = \begin{pmatrix} -40.89 & 0.4 & -17.87 & 34.01 & -14.28 \\ 0.4 & -37.36 & -0.43 & 14.32 & 45.74 \\ -17.87 & -0.43 & 66.18 & -19.62 & 35.26 \\ 34.01 & 14.32 & -19.62 & 66.49 & 26.71 \\ -14.28 & 45.74 & 35.26 & 26.71 & -295.49 \end{pmatrix}.$$

Another tight-binding model includes both Co d atoms and O p orbitals. There are in total 34 orbitals. The on-site Hamiltonian for both d orbitals and p orbitals, as well as the direct hopping between d-d orbitals and the hopping between p-d orbitals, are given as

$$H_d^{34} = \begin{pmatrix} 3721.77 & 0 & 1.01 & 3.83 & -4.83 \\ 0 & 3721.77 & 5 & -3.37 & -1.63 \\ 1.01 & 5 & 3543.68 & 10.93 & 10.93 \\ 3.83 & -3.37 & 10.93 & 3543.68 & 10.93 \\ -4.83 & -1.63 & 10.93 & 10.93 & 3543.68 \end{pmatrix},$$

$$T_{dd}^{34} = \begin{pmatrix} -28.31 & -9.34 & -5.14 & 5.08 & -22.57 \\ -9.34 & -45.42 & 12.23 & 0.92 & -104.37 \\ -5.14 & 12.23 & 82.14 & -108.02 & 14.97 \\ 5.08 & 0.92 & -108.02 & 64.46 & -9.19 \\ -22.57 & -104.37 & 14.97 & -9.19 & -249.37 \end{pmatrix},$$

$$H_p^{34} = \begin{pmatrix} 43.28 & -890.74 & -890.74 \\ -890.74 & 43.28 & -890.74 \\ -890.74 & -890.74 & 43.28 \end{pmatrix},$$

$$T_{dp}^{34} = \begin{pmatrix} -1151.92 & -61.22 & 175.07 \\ 653.14 & 36.17 & -133.84 \\ 5.62 & -40.96 & 1.85 \\ 163.59 & 32.32 & 625.23 \\ 11.17 & 691.32 & 28.09 \end{pmatrix}.$$

APPENDIX C: J, K, AND Γ INTERACTIONS FOR AN IDEAL OCTAHEDRAL CAGE

For the Heisenberg and Kitaev interactions the intersite exchange paths are listed in Table IV. There are several paths, and a detailed balance among them may change the order of the dominant interactions. On the other hand, for the Γ interaction from the intersite processes, there are only two contributions from t_1t_2 and t_2t_3.

TABLE IV. Intersite U exchange interactions for ideal case.

	J	K
t_1^2	$\frac{1}{486}\left(-\frac{171}{U-3J_H}+\frac{259}{U+J_H}+\frac{44}{U+4J_H}\right)$	$\frac{1}{243}\left(\frac{45}{U-3J_H}+\frac{11}{U+J_H}+\frac{28}{U+4J_H}\right)$
t_2^2	$\frac{1}{54}\left(-\frac{21}{U-3J_H}+\frac{29}{U+J_H}+\frac{4}{U+4J_H}\right)$	$\frac{1}{243}\left(-\frac{81}{U-3J_H}+\frac{73}{U+J_H}-\frac{4}{U+4J_H}\right)$
t_3^2	$\frac{2}{243}\left(-\frac{27}{U-3J_H}+\frac{43}{U+J_H}+\frac{8}{U+4J_H}\right)$	$\frac{2}{81}\left(\frac{3}{U-3J_H}-\frac{7}{U+J_H}-\frac{2}{U+4J_H}\right)$
t_4^2	$\frac{100}{81(U+2J_H)}$	0
t_5^2	$\frac{100}{81(U+2J_H)}$	0
t_6^2	$\frac{5}{243}\left(-\frac{27}{U-3J_H+\Delta_c}+\frac{43}{U+J_H+\Delta_c}+\frac{8}{U+4J_H+\Delta_c}+\frac{24}{U+2J_H-\Delta_c}\right)$	$\frac{5}{243}\left(-\frac{9}{U-3J_H+\Delta_c}+\frac{1}{U+J_H+\Delta_c}-\frac{4}{U+4J_H+\Delta_c}-\frac{12}{U+2J_H-\Delta_c}\right)$
t_1t_3	$\frac{4}{243}\left(\frac{18}{U-3J_H}-\frac{8}{U+J_H}+\frac{5}{U+4J_H}\right)$	$\frac{1}{243}\left(-\frac{63}{U-3J_H}+\frac{31}{U+J_H}-\frac{16}{U+4J_H}\right)$
$\Gamma = \frac{4t_1t_2}{81}\left(\frac{3}{U-3J_H}-\frac{7}{U+J_H}-\frac{2}{U+4J_H}\right)+\frac{t_2t_3}{243}\left(-\frac{63}{U-3J_H}+\frac{31}{U+J_H}-\frac{16}{U+4J_H}\right)$		

The two-hole (denoted by the superscript $2h$) and cyclic exchange (superscript cyclic) processes are

$$
\begin{aligned}
J^{2h} = & \left[-\frac{80}{81}\frac{1}{(2\Delta_{pd}+U_p-3J_{Hp})} + \frac{304}{243}\frac{1}{(2\Delta_{pd}+U_p-J_{Hp})} + \frac{32}{243}\frac{1}{(2\Delta_{pd}+U_p+2J_{Hp})} \right] t_{pd\pi}^4 \left(\frac{1}{\Delta_{pd}^2}\right) \\
& + \left[-\frac{10}{27}\frac{1}{2\Delta_{pd}+U_p-3J_{Hp}+\Delta_c} + \frac{250}{243}\frac{1}{(2\Delta_{pd}+U_p-J_{Hp}+\Delta_c)} + \frac{80}{243}\frac{1}{(2\Delta_{pd}+U_p+2J_{Hp}+\Delta_c)^2} \right] \\
& \times t_{pd\pi}^2 t_{pd\sigma}^2 \left(\frac{1}{\Delta_{pd}} + \frac{1}{\Delta_{pd}+\Delta_c}\right)^2 \\
& + \left[-\frac{200}{81}\frac{1}{(2\Delta_{pd}+U_p-3J_{Hp}+2\Delta_c)} + \frac{200}{81}\frac{1}{(2\Delta_{pd}+U_p-J_{Hp}+2\Delta_c)} \right] t_{pd\sigma}^4 \left(\frac{1}{\Delta_{pd}+\Delta_c}\right)^2, \\
K^{2h} = & \left[\frac{40}{81}\frac{1}{(2\Delta_{pd}+U_p-3J_{Hp})} - \frac{56}{243}\frac{1}{(2\Delta_{pd}+U_p-J_{Hp})} + \frac{32}{243}\frac{1}{(2\Delta_{pd}+U_p+2J_{Hp})} \right] t_{pd\pi}^4 \left(\frac{1}{\Delta_{pd}^2}\right) \\
& + \left[-\frac{10}{81}\frac{1}{2\Delta_{pd}+U_p-3J_{Hp}+\Delta_c} - \frac{50}{243}\frac{1}{(2\Delta_{pd}+U_p-J_{Hp}+\Delta_c)} - \frac{40}{243}\frac{1}{(2\Delta_{pd}+U_p+2J_{Hp}+\Delta_c)} \right] \\
& \times t_{pd\pi}^2 t_{pd\sigma}^2 \left(\frac{1}{\Delta_{pd}} + \frac{1}{\Delta_{pd}+\Delta_c}\right)^2, \\
J^{\text{cyclic}} = & \left[\frac{2}{81\Delta_{pd}} \right] t_{pd\pi}^4 \left(\frac{1}{\Delta_{pd}^2}\right) + \left[-\frac{40}{81}\frac{1}{2\Delta_{pd}+\Delta_c} \right] t_{pd\pi}^2 t_{pd\sigma}^2 \left(\frac{1}{\Delta_{pd}} + \frac{1}{\Delta_{pd}+\Delta_c}\right)^2, \\
K^{\text{cyclic}} = & \left[-\frac{20}{81\Delta_{pd}} \right] t_{pd\pi}^4 \left(\frac{1}{\Delta_{pd}^2}\right) + \left[\frac{20}{81}\frac{1}{2\Delta_{pd}+\Delta_c} \right] t_{pd\pi}^2 t_{pd\sigma}^2 \left(\frac{1}{\Delta_{pd}} + \frac{1}{\Delta_{pd}+\Delta_c}\right)^2.
\end{aligned}
$$

[1] A. Kitaev, Anyons in an exactly solved model and beyond, Ann. Phys. (NY) **321**, 2 (2006).

[2] G. Jackeli and G. Khaliullin, Mott Insulators in the Strong Spin-Orbit Coupling Limit: From Heisenberg to a Quantum Compass and Kitaev Models, Phys. Rev. Lett. **102**, 017205 (2009).

[3] Y. Singh and P. Gegenwart, Antiferromagnetic Mott insulating state in single crystals of the honeycomb lattice material Na_2IrO_3, Phys. Rev. B **82**, 064412 (2010).

[4] Y. Singh, S. Manni, J. Reuther, T. Berlijn, R. Thomale, W. Ku, S. Trebst, and P. Gegenwart, Relevance of the Heisenberg-Kitaev Model for the Honeycomb Lattice Iridates A_2IrO_3, Phys. Rev. Lett. **108**, 127203 (2012).

[5] K. W. Plumb, J. P. Clancy, L. J. Sandilands, V. V. Shankar, Y. F. Hu, K. S. Burch, H.-Y. Kee, and Y.-J. Kim, α-$RuCl_3$: A spin-orbit assisted Mott insulator on a honeycomb lattice, Phys. Rev. B **90**, 041112(R) (2014).

[6] L. J. Sandilands, Y. Tian, K. W. Plumb, Y.-J. Kim, and K. S. Burch, Scattering Continuum and Possible Fractionalized Excitations in α-$RuCl_3$, Phys. Rev. Lett. **114**, 147201 (2015).

[7] H.-S. Kim, V. S. V., A. Catuneanu, and H.-Y. Kee, Kitaev magnetism in honeycomb $RuCl_3$ with intermediate spin-orbit coupling, Phys. Rev. B **91**, 241110(R) (2015).

[8] A. Banerjee, C. A. Bridges, J.-Q. Yan, A. A. Aczel, L. Li, M. B. Stone, G. E. Granroth, M. D. Lumsden, Y. Yiu, J. Knolle, S. Bhattacharjee, D. L. Kovrizhin, R. Moessner, D. A. Tennant, D. G. Mandrus, and S. E. Nagler, Proximate Kitaev quantum spin liquid behaviour in a honeycomb magnet, Nat. Mater. **15**, 733 (2016).

[9] X. Liu, T. Berlijn, W.-G. Yin, W. Ku, A. Tsvelik, Y.-J. Kim, H. Gretarsson, Y. Singh, P. Gegenwart, and J. P. Hill, Long-range magnetic ordering in Na_2IrO_3, Phys. Rev. B **83**, 220403(R) (2011).

[10] F. Ye, S. Chi, H. Cao, B. C. Chakoumakos, J. A. Fernandez-Baca, R. Custelcean, T. F. Qi, O. B. Korneta, and G. Cao, Direct evidence of a zigzag spin-chain structure in the honeycomb lattice: A neutron and x-ray diffraction investigation of single-crystal Na_2IrO_3, Phys. Rev. B **85**, 180403(R) (2012).

[11] J. A. Sears, M. Songvilay, K. W. Plumb, J. P. Clancy, Y. Qiu, Y. Zhao, D. Parshall, and Y.-J. Kim, Magnetic order in α-$RuCl_3$: A honeycomb-lattice quantum magnet with strong spin-orbit coupling, Phys. Rev. B **91**, 144420 (2015).

[12] R. D. Johnson, S. C. Williams, A. A. Haghighirad, J. Singleton, V. Zapf, P. Manuel, I. I. Mazin, Y. Li, H. O. Jeschke, R. Valentí, and R. Coldea, Monoclinic crystal structure of α-$RuCl_3$ and the zigzag antiferromagnetic ground state, Phys. Rev. B **92**, 235119 (2015).

[13] H. B. Cao, A. Banerjee, J.-Q. Yan, C. A. Bridges, M. D. Lumsden, D. G. Mandrus, D. A. Tennant, B. C. Chakoumakos, and S. E. Nagler, Low-temperature crystal and magnetic structure of α-$RuCl_3$, Phys. Rev. B **93**, 134423 (2016).

[14] H. Takagi, T. Takayama, G. Jackeli, G. Khaliullin, and S. E. Nagler, Concept and realization of Kitaev quantum spin liquids, Nat. Rev. Phys. **1**, 264 (2019).

[15] J. Chaloupka, G. Jackeli, and G. Khaliullin, Kitaev-Heisenberg Model on a Honeycomb Lattice: Possible Exotic Phases in Iridium Oxides A_2IrO_3, Phys. Rev. Lett. **105**, 027204 (2010).

[16] J. Chaloupka, G. Jackeli, and G. Khaliullin, Zigzag Magnetic Order in the Iridium Oxide Na_2IrO_3, Phys. Rev. Lett. **110**, 097204 (2013).

[17] J. G. Rau, Eric Kin-Ho Lee, and H.-Y. Kee, Generic Spin Model for the Honeycomb Iridates beyond the Kitaev Limit, Phys. Rev. Lett. **112**, 077204 (2014).

[18] J. G. Rau and H.-Y. Kee, Trigonal distortion in the honeycomb iridates: Proximity of zigzag and spiral phases in Na_2IrO_3, arXiv:1408.4811.

[19] H. Liu and G. Khaliullin, Pseudospin exchange interactions in d^7 cobalt compounds: Possible realization of the Kitaev model, Phys. Rev. B **97**, 014407 (2018).

[20] R. Sano, Y. Kato, and Y. Motome, Kitaev-Heisenberg Hamiltonian for high-spin d^7 Mott insulators, Phys. Rev. B **97**, 014408 (2018).

[21] H. Liu, J. Chaloupka, and G. Khaliullin, Kitaev Spin Liquid in 3*d* Transition Metal Compounds, Phys. Rev. Lett. **125**, 047201 (2020).

[22] M. Songvilay, J. Robert, S. Petit, J. A. Rodriguez-Rivera, W. D. Ratcliff, F. Damay, V. Balédent, M. Jiménez-Ruiz, P. Lejay, E. Pachoud, A. Hadj-Azzem, V. Simonet, and C. Stock, Kitaev interactions in the Co honeycomb antiferromagnets $Na_3Co_2SbO_6$ and $Na_2Co_2TeO_6$, Phys. Rev. B **102**, 224429 (2020).

[23] W. Yao and Y. Li, Ferrimagnetism and anisotropic phase tunability by magnetic fields in $Na_2Co_2TeO_6$, Phys. Rev. B **101**, 085120 (2020).

[24] H. K. Vivanco, B. A. Trump, C. M. Brown, and T. M. McQueen, Competing antiferromagnetic-ferromagnetic states in a d^7 Kitaev honeycomb magnet, Phys. Rev. B **102**, 224411 (2020).

[25] X. Zhang, Y. Xu, T. Halloran, R. Zhong, R. J. Cava, C. Broholm, N. Drichko, and N. P. Armitage, A magnetic continuum observed by terahertz spectroscopy in a quantum spin liquid candidate $BaCo_2(AsO_4)_2$, Nat. Mater. **22**, 58 (2023).

[26] C. Kim, J. Jeong, G. Lin, P. Park, T. Masuda, S. Asai, S. Itoh, H.-S. Kim, H. Zhou, J. Ma, and J.-G. Park, Antiferromagnetic Kitaev interaction in $J_{\text{eff}} = \frac{1}{2}$ cobalt honeycomb materials $Na_3Co_2SbO_6$ and $Na_2Co_2TeO_6$, J. Phys.: Condens. Matter **34**, 045802 (2022).

[27] W. Chen, X. Li, Z. Hu, Z. Hu, L. Yue, R. Sutarto, F. He, K. Iida, K. Kamazawa, W. Yu, X. Lin, and Y. Li, Spin-orbit phase behavior of $Na_2Co_2TeO_6$ at low temperatures, Phys. Rev. B **103**, L180404 (2021).

[28] C. H. Lee, S. Lee, Y. S. Choi, Z. H. Jang, R. Kalaivanan, R. Sankar, and K.-Y. Choi, Multistage development of anisotropic magnetic correlations in the Co-based honeycomb lattice $Na_2Co_2TeO_6$, Phys. Rev. B **103**, 214447 (2021).

[29] A. M. Samarakoon, Q. Chen, H. Zhou, and V. O. Garlea, Static and dynamic magnetic properties of honeycomb lattice antiferromagnets $Na_2M_2TeO_6$, M = Co and Ni, Phys. Rev. B **104**, 184415 (2021).

[30] A. L. Sanders, R. A. Mole, J. Liu, A. J. Brown, D. Yu, C. D. Ling, and S. Rachel, Dominant Kitaev interactions in the honeycomb materials $Na_3Co_2SbO_6$ and $Na_2Co_2TeO_6$, Phys. Rev. B **106**, 014413 (2022).

[31] C. Kim, H.-S. Kim, and J.-G. Park, Spin-orbital entangled state and realization of Kitaev physics in 3d cobalt compounds: A progress report, J. Phys.: Condens. Matter **34**, 023001 (2022).

[32] H. Yang, C. Kim, Y. Choi, J. H. Lee, G. Lin, J. Ma, M. Kratochvílová, P. Proschek, E.-G. Moon, K. H. Lee, Y. S. Oh, and J.-G. Park, Significant thermal Hall effect in the 3*d* cobalt Kitaev system $Na_2Co_2TeO_6$, Phys. Rev. B **106**, L081116 (2022).

[33] S. Das, S. Voleti, T. Saha-Dasgupta, and A. Paramekanti, XY magnetism, Kitaev exchange, and long-range frustration in the $J_{\text{eff}} = \frac{1}{2}$ honeycomb cobaltates, Phys. Rev. B **104**, 134425 (2021).

[34] P. A. Maksimov, A. V. Ushakov, Z. V. Pchelkina, Y. Li, S. M. Winter, and S. V. Streltsov, Ab initio guided minimal model for the "Kitaev" material $BaCo_2(AsO_4)_2$: Importance of direct hopping, third-neighbor exchange, and quantum fluctuations, Phys. Rev. B **106**, 165131 (2022).

[35] S. M. Winter, Magnetic couplings in edge-sharing high-spin d^7 compounds, J. Phys. Mater. **5**, 045003 (2022).

[36] T. Halloran, F. Desrochers, E. Z. Zhang, T. Chen, L. E. Chern, Z. Xu, B. Winn, M. K. Graves-Brook, M. B. Stone, A. I. Kolesnikov, Y. Qui, R. Zhong, R. Cava, Y. B. Kim, and C. Broholm, Geometrical frustration versus Kitaev interactions in $BaCo_2(AsO_4)_2$, Proc. Natl. Acad. Sci. USA **120**, e2215509119 (2023).

[37] H. S. Nair, J. M. Brown, E. Coldren, G. Hester, M. P. Gelfand, A. Podlesnyak, Q. Huang, and K. A. Ross, Short-range order in the quantum XXZ honeycomb lattice material $BaCo_2(PO_4)_2$, Phys. Rev. B **97**, 134409 (2018).

[38] J. Kanamori, Electron correlation and ferromagnetism of transition metals, Prog. Theor. Phys. **30**, 275 (1963).

[39] S. Sugano, *Multiplets of Transition-Metal Ions in Crystals* (Academic Press, New York, 2014).

[40] Y. Wang, G. Fabbris, M. Dean, and G. Kotliar, Edrixs: An open source toolkit for simulating spectra of resonant inelastic x-ray scattering, Comput. Phys. Commun. **243**, 151 (2019).

[41] M. E. A. Coury, S. L. Dudarev, W. M. C. Foulkes, A. P. Horsfield, P.-W. Ma, and J. S. Spencer, Hubbard-like Hamiltonians for interacting electrons in *s*, *p*, and *d* orbitals, Phys. Rev. B **93**, 075101 (2016).

[42] X. Liu, D. Churchill, and H.-Y. Kee, Theoretical analysis of single-ion anisotropy in d^3 Mott insulators, Phys. Rev. B **106**, 035122 (2022).

[43] H. Liu, Towards Kitaev Spin Liquid in 3d Transition Metal Compounds, Int. J. Mod. Phys. B **35**, 2130006 (2021).

[44] P. Fazekas, *Lecture Notes on Electron Correlation and Magnetism* (World Scientific, Singapore, 1999).

[45] G. Kresse and J. Hafner, *Abinitio* molecular dynamics for liquid metals, Phys. Rev. B **47**, 558 (1993).

[46] P. E. Blöchl, Projector augmented-wave method, Phys. Rev. B **50**, 17953 (1994).

[47] J. P. Perdew, K. Burke, and M. Ernzerhof, Generalized Gradient Approximation Made Simple, Phys. Rev. Lett. **77**, 3865 (1996).

[48] G. Pizzi *et al.*, WANNIER90 as a community code: New features and applications, J. Phys.: Condens. Matter **32**, 165902 (2020).

[49] J. Chaloupka and G. Khaliullin, Hidden symmetries of the extended Kitaev-Heisenberg model: Implications for the honeycomb-lattice iridates A_2IrO_3, Phys. Rev. B **92**, 024413 (2015).

[50] J. Cen and H.-Y. Kee, Strategy to extract Kitaev interaction using symmetry in honeycomb Mott insulators, Commun. Phys. **5**, 119 (2022).

[51] P. P. Stavropoulos, X. Liu, and H.-Y. Kee, Magnetic anisotropy in spin-3/2 with heavy ligand in honeycomb Mott insulators: Application to CrI_3, Phys. Rev. Res. **3**, 013216 (2021).